J Mater Sci (2011) 46:6910–6915
DOI 10.1007/s10853-011-5656-8

The isochronal $\delta \rightarrow \gamma$ transformation of high Cr ferritic heat-resistant steel during cooling

Qiuzhi Gao · Yongchang Liu · Xinjie Di · Zhizhong Dong · Zesheng Yan

Received: 24 March 2011 / Accepted: 24 May 2011 / Published online: 4 June 2011

Abstract Thermal simulation technology was employed to investigate phase transformation in heat-affected zones (HAZ) of high Cr ferritic heat-resistant steel. The simulated continuous cooling transformation diagram was established based on the experimental results obtained from different cooling rates in the range of 0.02–60 °C/s. A theoretical model considering the site saturation nucleation at grain boundaries has been applied to calculate the austenite fraction as a function of cooling rate. It is found that both the austenite fraction and grain size decrease with the increase of cooling rates. The calculated results are mostly consistent with the experimental data.

Introduction

The high Cr ferritic heat-resistant steel is widely used in critical components of power plant for its high temperature stability, high creep strength, low thermal expansion coefficient, and outstanding corrosion resistance [1–3]. In consideration of the importance in fabrication of components, the weldability of the steel as a very important part must be well investigated to attain ideal condition. The performance of the steel can be significantly influenced by the welding-induced phase transformation, and so understanding the evolution of microstructure during welding is important to predict the final microstructure after welding treatment.

Q. Gao · Y. Liu · X. Di (✉) · Z. Dong · Z. Yan
School of Material Science and Engineering, Tianjin Key Laboratory of Advanced Jointing Technology, Tianjin University, Tianjin 300072, People's Republic of China
e-mail: licmtju@163.com

In the heat-affected zone (HAZ), the phase transformation is strongly dependent on the specific welding thermal cycles. The microstructure undergoes both different heat input and rapid cooling conditions which vary at different locations and drives the phase transformations to different levels. It is very important for high Cr ferritic heat-resistant steel to achieve uniform final microstructure in service. However, the HAZ always exhibits abnormal microstructure, especially the existing of δ-ferrite, which will induce deteriorating properties. The final microstructure can not provide any information about how it is obtained or how phase transformations take place during specific thermal cycles, particularly under cooling condition. The phase transformation under realistic welding procedures is inherently very difficult to be understood, thus thermal simulation of HAZ transformation behavior is widely used in previous investigations [4–8].

Since welding thermal simulation can approximately reflect the progress of phase transformations, the kinetics of $\delta \rightarrow \gamma$ transformations during cooling is an useful analysis to understand and predict the final microstructure. Several researchers [4–8] have analyzed the kinetics of $\delta \rightarrow \gamma$ transformations in the HAZ of duplex stainless steel using a model based upon grain boundary nucleation theory to calculate phase transformation during cooling. In their calculations, it was hypothesized that only the nitrogen diffusion controls phase transformations. There are two points supporting that the diffusion of nitrogen would play a predominant role in the microstructural formation of HAZ. First of all, additional nitrogen would be introduced in the HAZ during welding (nitrogen adsorption from the atmosphere at high temperature). Second, carbon has been used mainly to form carbides with other alloying substitutional components (precipitation strengthening) during production. Most of those formed carbides can not be

dissolved when the steel specimen was shortly heated up into the austenite region, and even those dissolved carbon would be used to reform carbides upon subsequent cooling. Hence, only the diffusion of nitrogen was considered for the kinetic analysis of the HAZ.

In this article, the grain boundary nucleation model was employed in the thermal simulation of high Cr ferritic heat-resistant steel to establish the relationship between austenite fractions and cooling rates. The simulated continuous cooling transformation (SHCCT) diagram of HAZ was established and the effect of cooling rate on austenite grain size was also studied.

Experimental details

The experimental high Cr ferritic heat-resistant steel was produced by Tian Jin Piping (Group) Corporation with the chemical composition given in Table 1. Cylindrical specimens, ϕ 9 × 100 mm, were machined from the rolled pipe with a thickness of 9 mm. The thermal simulation procedures were performed on heat simulator with programmed temperature cycles (see Fig. 1). Different cooling rates in the range of 0.02–60 °C/s were adopted for each measurement.

The austenite volume fractions of each measurement can be obtained by computer-aided software based on the optical microstructural images adopting standard metallographic preparation techniques. The number of measurements adopted for calculation is not less than 25 pictures. Metallographic grain size measurements were performed by Digital Micrograph Software according to the observation of optical images. The grain size was quantified as the equivalent diameter, i.e., the diameter of a circular disk with the same area as the grain [9].

Theoretical model

The austenite fraction is determined by assuming that austenite nucleates at the grain boundaries of δ-ferrite (site saturation), and grows up in a planar mode. Hence, the kinetics of grain boundary nucleation can be described by a model proposed by Cahn [10]

$$X = 1 - \exp[(-b_s^{-1/3})f(a_s)] \tag{1}$$

where X is the volume fraction, $b_s = \frac{I_s}{8S^3G}$, $f(a_s) = a_s \int_0^1 \left(1 - e^{-\pi a_s^3[\frac{1-x^3}{3} - x^2(1-x)]}\right) dx$ and $f(a_s)$ can be calculated

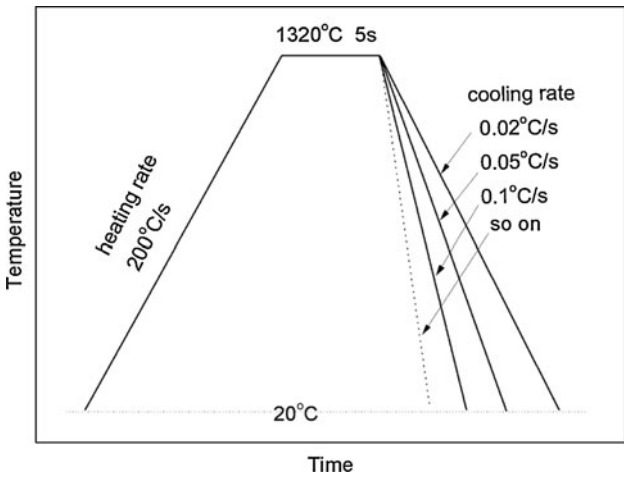

Fig. 1 Schematic diagram of experimental heat-treatment process

numerically by Simpson's rule. I_s is the grain boundary nucleation frequency per unit area (m^{-2}). S is the grain boundary area per unit volume which can be calculated as [10]:

$$S = \frac{3.35}{d_{gs}} \tag{2}$$

where d_{gs} is the grain size set to 65 μm based on the experimental results. Site saturation nucleation is taken into account, and G is the diffusion-controlled planar growth velocity which can be determined by a quasi-stationary model [4–8]:

$$G = \frac{D_N(T)}{r} \cdot \frac{\Omega^2}{2(1-\Omega)} \tag{3}$$

where T is the temperature, $D_N(T)$is the nitrogen diffusion coefficient, and r is the thickness of the grain boundary film. For a constant cooling rate c, r can be written as:

$$r = \sqrt{r_0 + \frac{D_N(T) \cdot \Omega(T)^2}{2(1-\Omega(T))} \cdot \frac{dT}{c}} \tag{4}$$

where the nucleus size r_0 at the beginning of the transformation is zero when a nucleation of site saturation is adopted.

$$\Omega(T) = \frac{N_S - N_{\delta/\gamma}}{N_{\gamma/\delta} - N_{\delta/\gamma}} \tag{5}$$

where N_S is the nitrogen concentration of steel, $N_{\delta/\delta\gamma.\gamma}$ is the nitrogen concentration of δ phase in equilibrium with γ phase, $N_{\gamma/\gamma\delta.\delta}$ is the nitrogen concentration of γ phase in

Table 1 Chemical compositions of high Cr ferritic steel (in mass)

Element	C	Si	Mn	Cr	Mo	W	V	Nb	N	Co	B	Ti	Al
Wt%	0.05	0.21	0.44	9.81	0.43	1.73	0.22	0.07	0.03	1.21	0.0045	<0.01	0.014

equilibrium with δ phase. The equilibrium nitrogen concentration can be approximated by the equilibrium solid solubility of nitrogen in iron according to thermo-calc calculation: $N_{\delta/\gamma} = 10^{-1638/T-1.0259}$ (wt%), $N_{\gamma/\delta} = 10^{791/T-2.195}$ (wt%). For the diffusion coefficient of nitrogen in the explored steel is not readily available, it was approximately estimated by the diffusion coefficient of nitrogen in iron as [11]:

$$D_{\mathrm{N}}(T) = 0.0078\exp\left(-\frac{79100}{RT}\right) \tag{6}$$

where R is the Boltzmann constant.

During cooling, the austenite starts to transform at higher temperature T_{start} and finishes at T_{fin}, so the thickness of grain boundary film can be calculated as:

$$r^2 = \int_{T_{\mathrm{fin}}}^{T_{\mathrm{start}}} \frac{D_{\mathrm{N}}(T)\cdot\Omega(T)^2}{2(1-\Omega(T))}\cdot\frac{\mathrm{d}T}{c}. \tag{7}$$

Substituting Eqs. 2–7 into 1, the austenite fraction can be determined when the parameters, N_{S}, $N_{\delta/\delta\gamma.\gamma}$, $N_{\gamma/\gamma\delta.\delta}$, $D_{\mathrm{N}}(T)$, I_s, and d_{gs}, are known.

Results and discussion

Figure 2 illustrates the obtained SHCCT diagram for the explored high Cr heat-resistant ferritic steel. The measured curves under different cooling rates from 7.5 to 15,000 s in the diagram represent different cooling time of HAZ. Just austenite and martensite transformations were found, whereas no ferrite transformation was observed in the SHCCT diagram, for there was no ferrite dilatometer curve of thermal simulation. The martensite transformation region from 410 °C (M_s) to 350 °C (M_f) at all cooling rates means the stability of martensite transformation. The experimentally determined M_s temperature point is in agreement with the calculated M_s temperature (about 406 °C) based on the empirical expression in Ref. [12]. Both A_{c1} and A_{c3} temperature points are higher than the austenization temperatures of the matrix materials. It can be attributed to the delay of austenite transformation due to superheating under fast heating rate of 200 °C/s, and the specific simulated HAZ peak temperature (1320 °C).

Figure 3 represents optical microstructures of the explored high Cr ferritic steel etched by a solution of 2.5 g $FeCl_3$ + 2.5 g $CuCl_2$ + 40 mL HCl + 120 mL H_2O after experiencing heat treatment under various cooling rates. It can be found that the room temperature microstructures are consisted of martensite and δ-ferrite. The δ-ferrite may have formed when the specimen was held at the peak temperature (1320 °C). Some coarse δ-ferrite exist in the steel specimens with slow cooling rates, and then absent when the cooling rate is above 10 °C/s. With increasing the cooling rate, it is also observed that the number of coarse precipitates decreases gradually, and finally disappears while cooling rate increases to 10 °C/s. What is more, the shape of ferrite changes from slender strip to polygon, as well as its fraction increases with the increase of cooling rates.

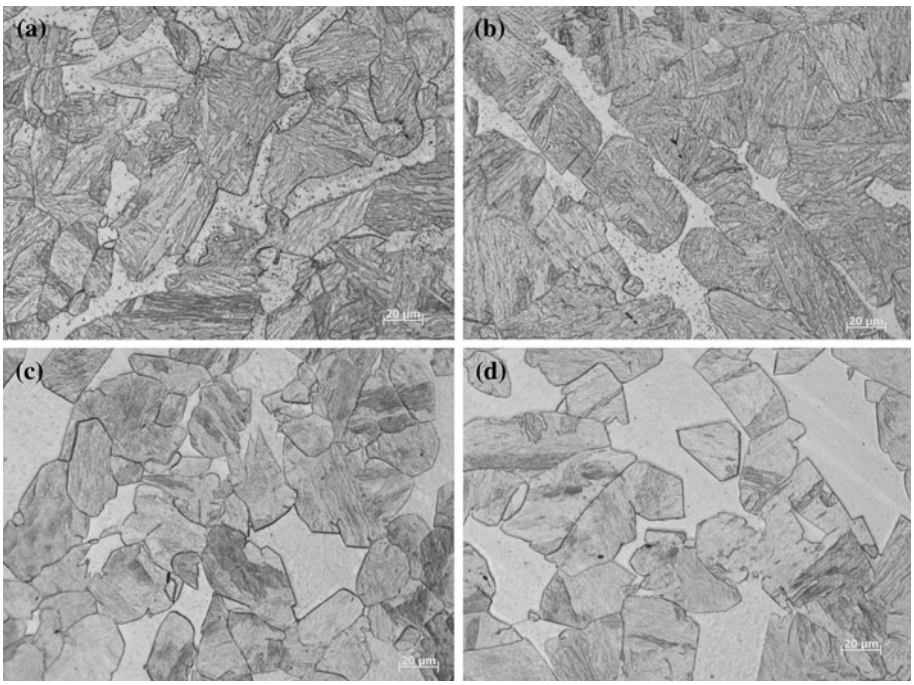

Fig. 2 Optical images of the explored high Cr ferritic steel formed via various cooling rates applied **a** 1 °C/s, **b** 5 °C/s, **c** 10 °C/s, **d** 60 °C/s

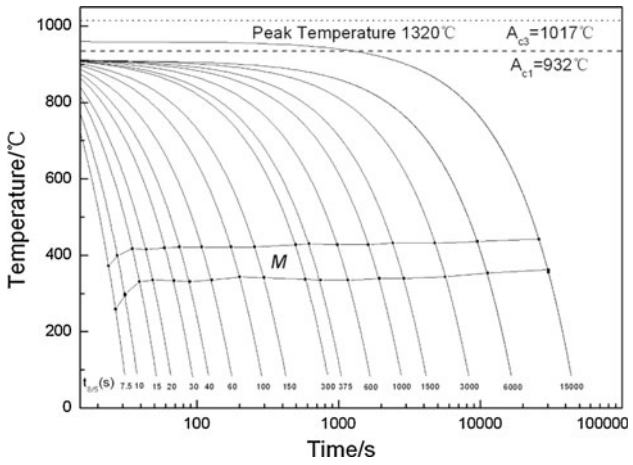

Fig. 3 SHCCT diagram of the explored high Cr ferritic steel

Figure 4 represents the diagram of transformed phase as a function of net chromium equivalent (NCE) at medium and high temperatures [13]. The value of NCE for the experimental steel that was calculated based on an equation in Ref. [14] is about 12.203, and it is marked in Fig. 4. For the given value of NCE, the region of simulated HAZ at the peak temperature is well with in the δ-ferrite phase field. That is to say, only δ-ferrite phase exists while simulated heating to the peak temperature. In addition, the austenite transformation below the peak temperature also can not occur completely, and thus lead to ferrite + austenite duplex phase coexisting. In-depth analyzing of Fig. 4, it could be considered that the complete austenization can not occur only if the value of NCE is less than 12, or else, a duplex structure of ferrite + austenite will form.

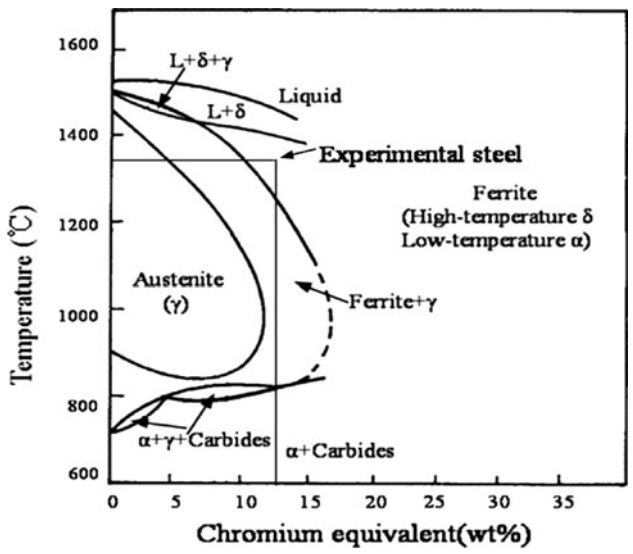

Fig. 4 Equilibrium diagram showing the dependence of the existence of various phases on chromium equivalent [13]. The experimental high Cr ferritic steel is indicated by the *vertical line*

Maehara [15] had shown that a lamellar/cellular structure of $M_{23}C_6$ and austenite initiated nucleating at the interface of δ-ferrite/matrix austenite, then $M_{23}C_6$ particles grew into δ-ferrite in AISI 304L stainless steel, whereas no $M_{23}C_6$ that separated out in the δ-ferrite grains was found. As we discussed above, ferrite and austenite are concomitant at high temperature region, but δ-ferrite may be the only phase at the peak temperature (1320 °C) for the explored high Cr ferritic heat-resistant steel. There may be another possibility that a new austenite embryo will nucleate at the δ-ferrite matrix and then grow up to an austenite grain. It means that δ-ferrite will directly transform into austenite, with the temperature decreasing. Correlational research [16, 17] has illustrated that the migration of the δ/γ interface boundary into the ferrite phase region resulted from the nucleation and growth of the $M_{23}C_6$ carbides with patterns of "lamellar" and "larva". The transformation from δ-ferrite to austenite becomes less sufficiently followed by the heightening of cooling rate, and that leads to reduction in the amount of austenite transformation. The interface boundary of δ-ferrite/new austenite will continuously migrate into δ-ferrite, and then new austenite grain grows up.

It is proved that the high temperature phases during/above austenization temperature interval are austenite + ferrite duplex phases based on the above analysis, but the ferrite → austenite phase transformation kinetic still need to be analyzed based on grain boundaries nucleation and growth model. Since the initial microstructure of the material at the peak temperature region is initially δ-ferrite as we discussed above, it is reasonable to assume that the initial number of austenite nuclei at the beginning of the transformation is zero. Upon subsequent cooling, the austenite will nucleate immediately at the boundaries of δ-ferrite when the specimen temperature enters into austenitization region. Hence, the case is considered where there already is a number of pre-existing nuclei (supercritical particles of the new phase) at $t = 0$ and the further nucleation rate is zero [18]. The subsequent phase transformation simply involves the re-constructive thickening of the austenite layer. Furthermore, without consideration of the redistribution of other metallic constituents, the $\delta \rightarrow \gamma$ phase transformation is assumed to be controlled only by the diffusion of nitrogen in the δ-ferrite. So the analysis is based on the assumption that the transformation is driven by nitrogen distribution and that other metallic element compositions of ferrite and austenite are the same. The kinetic of $\delta \rightarrow \gamma$ phase transformation can be calculated based on the theoretical expression.

The experimental results of austenite fraction and grain size in the explored high Cr ferritic heat-resistant steel specimens are shown in Fig. 5 and collected in Table 2. As compared to the calculated values of austenite fraction, it is

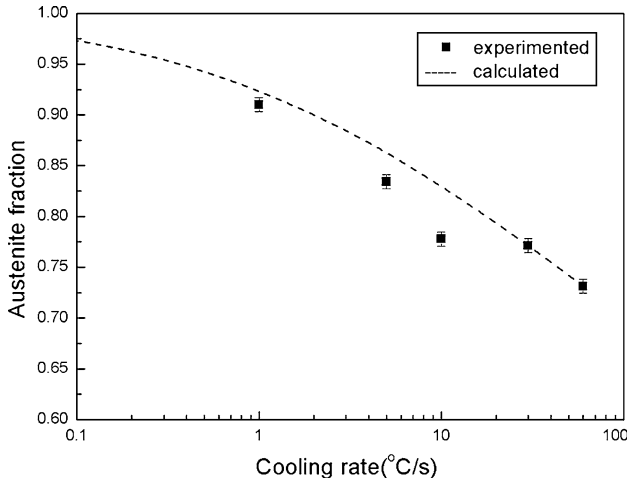

Fig. 5 The experimental and calculated austenite fractions of the explored high Cr ferritic steel as a function of cooling rates applied

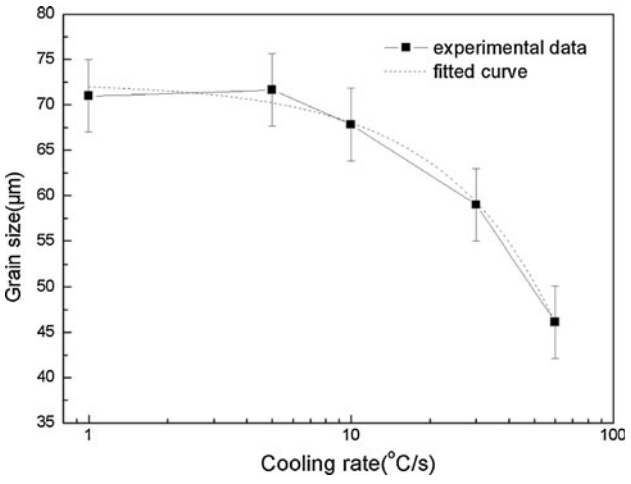

Fig. 6 The experimental and calculated grain sizes of the austenite in the explored high Cr ferritic steel as a function of cooling rates applied

Table 2 The measured values of austenite fractions and grain sizes as a function of cooling rates in the explored high Cr ferritic steel

Cooling rate (°C/s)	Grain size (μm)	Austenite fraction (%)
1	70.97	88.01
5	71.62	83.45
10	67.82	77.58
30	63.56	77.14
60	48.91	73.13

observed that the austenite fraction varies clearly with cooling rate. The transformed amounts decrease with applied cooling rate increasing, which is confirmed by both the experimental results and the calculated curve. In Fig. 5, it is also found that the calculated curve is fundamental agreement with experimental data with comparison. This can be considered that the assumption that the transformation is controlled by the nitrogen diffusion from a site-saturated ferrite to the reforming austenite can be approximately applicable for the experimental steel.

The average grain size of austenite is presented as a function of cooling rate in Fig. 6. When it is heated to austenitization temperature, austenite starts to nucleate and then grow to a certain size relating to austenitization time. The applied cooling rate is inversely proportional to the austenitization holding period. That is, the lower the applied cooling rate, the longer the austenitization time. Figure 6 represents that the measured austenite grain sizes of the explored steel specimens as a function of cooling rates. The grain size of the specimen with lowest cooling rate (1 °C/s) is about 70 μm, while it is about 48 μm at a cooling rate of 60 °C/s. This phenomenon can be attributed to the variation in the austenitization time. Take the lowest and highest cooling rates as example, the austenitization time at 1 °C/s is about 90 s, but 1.5 s at 60 °C/s. There is sufficient time for the growth of the austenitic grain in the specimen cooled with 1 °C/s, whereas the time is not enough in the specimen cooled at 60 °C/s. The relationship between austenite grain size and cooling rate for the experimental high Cr ferritic heat-resistant steel can be fitted and described as:

$$d_\gamma = -0.44c + 72.41 \quad (8)$$

where c represents cooling rate and d_γ is austenite grain size.

Conclusions

1. Different cooling rates are performed to the high Cr ferritic heat-resistant steel, and only austenite and martensite transformations are found. The occurrence of austenite transformation is delayed due to the superheating effect from fast heating rate which leads to a rise of austenization temperature.
2. Both austenite and ferrite phases coexist when the high Cr ferritic heat-resistant steel was heated up into austenization temperature and ferrite will form at 1320 °C for the experimental steel. A correlation the austenite grain size and the cooling rate applied is established for the experimental steel. The austenite grain size decreases with the increase of the cooling rate applied.
3. Following the assumption that only the diffusion of nitrogen controls the phase transformation process, the experimental observation agrees mostly well with the prediction of the phase transformation model.

Acknowledgements The authors are grateful to the National Natural Science Foundation of China and Shanghai Baosteel Group Company (No. 50834011) for grant and financial support.

References

1. Mythili R, Thomas Paul V, Saroja S, Vijayalakshmi M, Raghunathan V (2003) J Nucl Mater 312:199
2. Klueh R, Nelson A (2007) J Nucl Mater 371:37
3. Jones W, Hills C, Polonis D (1991) Metal Mater Trans A 22:1049
4. Hertzman S, Brolund B, Ferreira P (1997) Metall Mater Trans A 28:277
5. Hemmer H, Grong (1999) Metall Mater Trans A 30:2915
6. Sieurin H, Sandstrm R (2006) Mater Sci Eng A 418:250
7. Zhang W, DebRoy T, Palmer T, Elmer J (2005) Acta Mater 53:4441
8. Zhang W, Elmer J, DebRoy T (2002) Scr Mater 46:753
9. Ferreira P, Hertzman S (1991) Proceedings of Duplex Stainless Steels '91, vol 2, Beaune, p 959
10. Cahn JW (1956) Acta Metall 4:449
11. Trivedi R, Pound G (1967) J Appl Phys 38:3569
12. Finkler H, Schirra M (1996) Steel Res 67:328
13. George G, Shaikh H, Parvathavarthini N, George R, Khatak H (2001) J Mater Eng Perform 10:460
14. Patriarca P, Harkness S, Duke J, Cooper L (1976) Nucl Technol 28:516
15. Maehara Y, Ohmori Y (1987) Metall Mater Trans A 18:663
16. Lee K, Cho H, Choi D (1999) J Alloys Compd 285:156
17. Jimenez J, Carsi M, Ruano O, Penalba F (2000) J Mater Sci 35:907. doi:10.1023/A:1004750424897
18. Liu F, Sommer F, Bos C, Mittemeijer E (2007) Int Mater Rev 52:193